Viral lysis alters the optical properties and biological availability of dissolved organic matter derived from picocyanobacteria *Prochlorococcus*

Xilin Xiao[1], Weidong Guo[1], Xiaolin Li[1], Chao Wang[1], Xiaowei Chen[1], Xingqin Lin[2], Markus G. Weinbauer[3], Qinglu Zeng[2,4], Nianzhi Jiao[1]*, Rui Zhang[1]*

1. State Key Laboratory of Marine Environmental Science, College of Ocean and Earth Sciences, Fujian Key Laboratory of Marine Carbon Sequestration, Xiamen University, Xiamen, China
2. Division of Life Science, The Hong Kong University of Science and Technology, Clear Water Bay, Hong Kong, China
3. Sorbonne Universités, UPMC, Université Paris 06, CNRS, Laboratoire d'Océanographie de Villefranche (LOV), Villefranche-sur-Mer, France
4. Department of Ocean Science, The Hong Kong University of Science and Technology, Clear Water Bay, Hong Kong, China

*Corresponding author: Nianzhi Jiao (jiao@xmu.edu.cn) or Rui Zhang (ruizhang@xmu.edu.cn)

Competing interests

The authors declare no competing interests.

Abstract

Phytoplankton contribute almost half of the world's total primary production. The exudates and viral lysates of phytoplankton are two important forms of dissolved organic matter (DOM) in aquatic environments and fuel heterotrophic prokaryotic metabolism. However, the effect of viral infection on the composition and biological availability of phytoplankton-released DOM is poorly understood. Here, we investigated the optical characteristics and microbial utilization of the exudates and viral lysates of the ecologically important unicellular picophytoplankton *Prochlorococcus*. Our results showed that *Prochlorococcus* DOM produced by viral lysis (Pro-vDOM) with phages of three different morphotypes (myovirus P-HM2, siphovirus P-HS2 and podovirus P-SSP7) had higher humic-like fluorescence intensities, lower absorption coefficients and higher spectral slopes compared to DOM exuded by *Prochlorococcus* (Pro-exudate). The results indicate that viral infection altered the composition of *Prochlorococcus*-derived DOM and might contribute to the pool of oceanic humic-like DOM. Incubation with Pro-vDOM resulted in a greater dissolved organic carbon (DOC) degradation rate and decreases in the absorption spectral slope and heterotrophic bacterial growth rate compared to incubation with Pro-exudate, suggesting that Pro-vDOM was more bioavailable compared to Pro-exudate. In addition, the stimulated microbial community succession trajectories were significantly different between the Pro-exudate and Pro-vDOM treatments, indicating that viral lysates play an important role in shaping the heterotrophic bacterial community. Our study demonstrated that viral lysis altered the chemical composition

and biological availability of DOM derived from *Prochlorococcus*, which is the numerically dominant phytoplankton in the oligotrophic ocean.

Importance

The unicellular picocyanobacterium *Prochlorococcus* is the numerically dominate phytoplankton in the oligotrophic ocean, contributing to the vast majority of marine primary production. *Prochlorococcus* releases a significant fraction of fixed organic matter into surrounding environment and supports a vital portion of heterotrophic bacterial activity. Viral lysis is an important biomass loss process of *Prochlorococcus*. Yet little is known about whether and how viral lysis affects *Prochlorococcus*-released dissolved organic matter (DOM). Our paper shows that viral infection alters the optical properties (such as the absorption coefficients, spectral slopes and fluorescence intensities) of released DOM and might contribute to a humic-like DOM pool and carbon sequestration in the ocean. Meanwhile, viral lysis also releases various intracellular labile DOM including amino acids, protein-like DOM and lower-molecular weight DOM, increases the bioavailability of DOM and shapes the successive trajectory of the heterotrophic bacterial community. Our study highlights the importance of viruses in impacting the DOM quality in the ocean.

Introduction

As the base of the marine food web, phytoplankton account for less than 1% of the photosynthetic biomass on Earth but contribute to almost half of the world's total primary production (1, 2). Large amounts of photosynthetically fixed organic matter are released into the surrounding seawater (3-5). It has been suggested that the rates of dissolved organic matter (DOM) production by phytoplankton will increase due to warmer, more acidic and more stratified conditions in the future ocean (6). Exudates and viral lysates are the two major sources of DOM released from phytoplankton. A significant proportion of phytoplankton are infected and lysed by viruses (5, 7, 8), thus releasing their cellular contents into the environment. Viral infections have been shown to restructure the fatty acids composition of *Emiliania huxleyi* (9). The production of DOM released by *Micromonas pusilla* was stimulated by viral infection, coupling with the change of DOM composition (4). Phytoplankton-derived DOM is highly bioavailable (10-12) and includes carbohydrates, amino acids (peptides and protein), carboxylic acids, lipids, and other cellular materials (such as pigments, polyphenols and trace metals) (3, 13-16). This DOM is primarily consumed by heterotrophic bacterioplankton, shapes the surrounding bacterial community structure and supports the function of the microbial loop (5, 17-20). Recently, Fang and colleagues (21) found that *Synechococcus* viral lysate may play a role as a source of organic nitrogen to regulate the transcription of the N-metabolism related genes of uninfected co-occurring phytoplankton.

In tropical and subtropical oligotrophic oceans, the unicellular

82 picocyanobacterium *Prochlorococcus* is the numerically dominant phytoplankton (22).
83 Its specific divinyl-chlorophyll *a* accounts for 30–60% of the total chlorophyll *a* in
84 subtropical oligotrophic oceans (23). Data from field surveys indicate that virus-
85 mediated mortality is responsible for up to 60% of *Prochlorococcus* cell loss (8, 24, 25)
86 and releases various DOM that serves as a large bioavailable carbon source in the vast
87 oligotrophic oceans. It is estimated that *Prochlorococcus* releases 9-24% of its daily
88 primary productivity as DOM into the surrounding environment, which supports a
89 large part of bacterial production in oligotrophic regions (3). The chemical molecular
90 analysis showed that the released DOM consists of low-molecular weight (LMW)
91 carboxylic acids, hydrocarbon, amino acids as well as small, nonpolar materials (3, 26,
92 27). However, the detailed effects of virus infection on the composition and microbial
93 utilization of DOM released from *Prochlorococcus* remain unstudied.

94 *Prochlorococcus* MED4 is an ecologically important high light-adapted
95 *Prochlorococcus* model strain. MED4 is distributed in the upper-middle euphotic zone
96 and achieves numerical dominance in well-mixed, nutrient-rich, high-latitude waters
97 (28). In this study, we conducted a microcosm experiment with DOM exuded by
98 *Prochlorococcus* during growing (Pro-exudate) and DOM released by lysis of
99 *Prochlorococcus* cells (Pro-vDOM) with infection of three lytic phages (myovirus P-HM2,
100 siphovirus P-HS2, and podovirus P-SSP7). We investigated the optical properties and
101 bioavailability of these different DOM types and the response of the microbial
102 community to a low dose of Pro-vDOM. In recent decades, it was demonstrated that
103 the absorption and fluorescence properties of DOM provide powerful indexes of DOM

characteristics (29), and they have been widely used in oceanographic studies (30, 31). The chemical composition of phytoplankton-derived DOM has been studied in detail using different mass spectrometry analyses (13, 15, 27). However, it is difficult to connect such analyses with oceanographic surveys that target the optical characteristics of DOM. By combining optical characterization with the biodegradation of *Prochlorococcus*-derived DOM, our study provides fundamental data to link laboratory analyses with large-scale oceanographic survey data. This work will help us understand the role of viral infection in the composition and biodegradability of phytoplankton-released DOM and improve the knowledge of the viral impact on ecology and biogeochemistry in the ocean.

Materials and Methods

Prochlorococcus DOM collection

Prochlorococcus MED4 and three phages with different morpholoies (myovirus P-HM2, siphovirus P-HS2 and podovirus P-SSP7) used in this work are routinely maintained at The Hong Kong University of Science and Technology (Table S1). Axenic *Prochlorococcus* strain MED4 was cultivated in eight one-litre polycarbonate bottles in Port Shelter (Hong Kong) seawater-based Pro99 medium (Pro-medium, 800 mL) with 50 µM $NaHPO_4$, 800 µM NH_4Cl, and trace metal mix (32) at 23 °C under constant cool white light (30 µE m^{-2} s^{-1}) (the method used for the axenicity tests for *Prochlorococcus* is shown in supplementary methods). After reaching the early-logarithmic growth phase (an abundance of ca. 10^8 cells mL^{-1}), six cultures were inoculated with myovirus P-HM2, siphovirus P-HS2, and podovirus P-SSP7 (ca. 10^9 particles mL^{-1}) at a ratio of

1:100 (volume/volume, corresponding MOI of 0.1). One week later, the cultures were filtered through 0.2 µm polycarbonate membranes (47mm, Millipore, USA). All filtrates and 2 L Pro-medium were stored in precombusted (450 °C for 6 h) 450 mL Boston round amber glass bottles (CNW, Germany) at 4 °C and used within three weeks. All filtration procedures were conducted at low pressure in a clean-hand bench. Here, we define P-HS2, P-HM2, and P-SSP7 lysates as virus-derived DOM (Pro-vDOM), the filtrate of *Prochlorococcus* culture without virus addition as Pro-exudate, Pro99 medium as Pro-medium and Pro-DOM as including both Pro-exudate and Pro-vDOM.

Before preforming dark incubation experiments, the DOC, CDOM, FDOM, and amino acid of the obtained DOM (Pro-DOM and Pro-medium) were measured (see below).

Dark incubation experiments

To examine the biodegradability of different DOMs derived from *Prochlorococcus* and the response of the oligotrophic bacterial community to these DOM, Pro-exudate and Pro-vDOM were added to and incubated with oligotrophic seawater (Figure S1). The surface water was collected from SEATS station (a well-investigated oligotrophic station) (33) at a 5 m depth in the South China Sea, using a rosette sampler with a conductivity–temperature–depth instrument, which yielded a recorded temperature of 29.5 °C and a salinity of 33.3, on 6 November, 2016. The seawater was filtered through a 0.8 µm-pore size membrane (the filter sets were prewashed with 20 L ultra-pure Milli-Q water, and the first 10 L seawater filtrate was discarded) to eliminate predators and particles intermediately and then dispatched into twelve 10 L acid-

prewashed polycarbonate carboys (wrapped with foil). The filtered seawater was amended with the following DOM sources: Pro-medium, Pro-exudate, and three *Prochlorococcus* virus lysates (namely, P-HS2 lysate, P-SSP7 lysate, and P-HM2 lysate). Studies have revealed that both DOM quality and quantity influence the microbial community (34, 35). A recent study showed that DOM quantity affects the bacterial community more than quality does (36). In this study, we added a low dose of DOM (8-15 µM) into each microcosm to avoid "shock" from DOM addition to microbial communities and to simulate the *in situ* conditions of the oligotrophic open ocean. Each DOM treatment had two replicates. Another two carboys contained 0.8 µm-filtered seawater sample without any treatment and were used as the controls for this experiment. During the experiment duration, samples were collected to determine the DOC concentration, CDOM, FDOM, amino acid, prokaryotic abundance, and bacterial community.

Dissolved organic carbon analysis

Dissolved organic carbon (DOC) samples were collected at 0, 6, 18, 36, 48, and 120 h with precombusted (450 °C, 6 h) glass pipettes and stored in precombusted (450 °C, 6 h) 40 mL amber vials at -20 °C until further analysis. Three subsamples were collected from each replicate. In this study, the incubation used 0.8 µm-filtered seawater, and the total organic carbon concentration was equivalent to the DOC concentration. Before analysis, the samples were thawed at room temperature and then acidified to pH < 2. The DOC concentration was measured using the high-temperature combustion method on a Shimadzu TOC-VCPH organic carbon analyser. Three to five injections of

150 µL were performed per sample until the coefficient of variation on the analysis of replicate measurements was approximately 2%. The concentrations were determined by subtracting the values from a blank of ultra-pure Milli-Q water and dividing the result by the slope of a daily standard curve made from potassium hydrogen phthalate. All samples were checked against deep-sea reference water and low-carbon water (provided by the Hansell Organic Biogeochemistry Laboratory, University of Miami, USA). The analytical precision was ± 1.7 µmol-C L^{-1} as indicated by the standard deviation of DOC measurement of deep-sea reference water (n=18).

Total amino acid analysis

Samples for total dissolved amino acid (TDAA) analysis were directly collected from the carboys with precombusted (450 °C, 6 h) glass pipettes and stored in 40 mL precombusted (450 °C, 6 h) amber glass vials at -20 °C until analysis. The measurement of TDAA used a previously established method (37), and the detailed method and settings referred to Li and colleagues (38). Thirteen amino acids, namely, aspartic acid (Asp), glutamic acid (Glu), serine (Ser), arginine (Arg), glycine (Gly), threonine (Thr), alanine (Ala), tyrosine (Tyr), valine (Val), phenylalanine (Phe), isoleucine (Ile), leucine (Leu), and γ-aminobutyric acid (GABA) were measured.

A 2 mL sub-sample was added to a screw-top tube spiked with 2 mL concentrated HCl (trace metal grade; Fisher, USA) and sealed under nitrogen before being hydrolyzed at 110 °C for 24 h. The hydrolysed samples were dried with ultra-pure nitrogen gas, dissolved in ultra-pure Milli-Q water, and finally spiked with aminoadipic acid. Then, 1 mL of the obtained sample was transferred to a 2-mL vial and then reacted with 100

192 µL of o-phthaldialdehyde (OPA) solution at room temperature for 2 min. A 20 µL
193 aliquot was injected into an HPLC system coupled with a fluorescence detector
194 (Shimadzu RF-20A) with excitation and emission wavelengths of 330 nm and 418 nm,
195 respectively. The separation of amino acids was accomplished using a reverse-phase
196 C18 column (Inert Sustain, 250×4.6 mm, particle size 5 µm) at a flow rate of 1.0 mL
197 min^{-1}. Mobile phase A consisted of 0.04 M potassium phosphate monobasic buffer
198 with 1% tetrahydrofuran, and the pH was adjusted to 6.2 with potassium hydroxide.
199 Mobile phase B consisted of HPLC-grade methanol, acetonitrile and ultra-pure water
200 mixed at a volume ratio of 4.5:4.5:1. The elution gradient (38) was performed over 73
201 min. The relative standard deviation of triplicate analyses was < 3%. Ultra-pure Milli-Q
202 water was used as the blank for every measurement batch. The mean peak areas of
203 each amino acid in the blanks were subtracted from the corresponding peaks of all
204 samples. The blanks were generally less than 2% of the sample signals measured in
205 this research.

206 **CDOM absorption, EEM measurement and PARAFAC modelling**

207 CDOM and FDOM sampling were performed at 0, 18, 36, 48, 72, 96, and 120 h.
208 All CDOM and FDOM samples were kept frozen (-20 °C) until further analysis. Storing
209 CDOM samples at -20 °C is a commonly used method for CDOM analyses, and a
210 number of marine DOM studies show the minimal effects from freezing/thawing on
211 DOM optical properties (39, 40). Ultra-pure Milli-Q water was used as the absorbance
212 and fluorescence blank. DOM absorption was measured as previously described (41).
213 Namely, the absorption scans ranged from 240 to 800 nm at 1 nm intervals using a

214 2300 UV-Visible spectrophotometer (Techcomp, China) with a 10 cm-path length
215 quartz cell at constant room temperature. Ultra-pure water was measured every 3
216 samples to detect and adjust for possible instrument drift. After subtracting the
217 average absorption value between 700 nm and 750 nm, absorbance values were
218 converted to Naperian absorbance coefficients using the following equation:

219 $$a = 2.303A/L$$

220 where a is the Napierian absorption coefficient (m^{-1}), A is the absorbance measured
221 by the spectrophotometer, and L is the path length (m). The spectral slope over the
222 wavelength range from 275 to 295 nm ($S_{275–295}$) was calculated by linear regression of
223 natural log-transformed absorption spectra (42). Helms and colleagues (42)
224 demonstrated that the $S_{275-295}$ can be related to the relative molecular weight of DOM,
225 and high $S_{275-295}$ values typically indicate LMW DOM.

226 Fluorescence measurements were analysed as previously described (41). Briefly,
227 EEMs were obtained using a Cary Eclipse (Varian, Australia) fluorimeter equipped with
228 a 150 W Xe arc lamp. The configuration included excitation from 250 to 450 nm in 5
229 nm intervals with acquisition from 280 to 600 nm at 2 nm intervals and 10 nm and 5
230 nm slit widths on the excitation and emission modes, respectively. The scan speed was
231 1920 nm min^{-1}, with the photomultiplier voltage set to 800 V. The EEMs of the samples
232 were blank corrected and Raman-normalized using ultra-pure Milli-Q water EEMs
233 scanned on the same day. In total, 168 EEM spectra were modelled using parallel factor
234 analysis (PARAFAC) with MATLAB 7.5 and the DOMFluor toolbox (43). Split-half
235 validation was used to determine the number of fluorescent components. The

fluorescence intensity of each fluorescent component was evaluated using the maximum fluorescence. EEM maps of *Prochlorococcus*-derived DOM were obtained after subtracting the blank and normalizing to the ultra-pure Milli-Q water Raman peak scanned on the same day. The fluorescent components of the obtained *Prochlorococcus*-derived DOM stocks were obtained by the traditional "peak-picking" method (44).

Prokaryotic abundance analysis

The prokaryotic abundance was determined at 0, 6, 12, 18, 24, 36, 48, 72, 96 and 120 h with the established methods (45). At each sampling time, 1.8 mL subsamples were fixed with a final concentration of 0.5% glutaraldehyde for 15 min in the dark, flash-frozen in liquid nitrogen and stored at -80 °C until analysis. Before analysis, the frozen prokaryotic abundance samples were thawed in a 37 °C bath. Then, 990 µL samples were stained with 10 µL SYBR Green I (Sigma-Aldrich, St. Louis, MO) for 15 min in the dark, and 10 µL 1 µm calibration beads (BD Bioscience) were added as reference before counting by flow cytometer (BD Accuri C6, USA), and prokaryotes were identified in plots of red fluorescence vs. green fluorescence. Autotrophic picoplankton abundance were analysed on a BD FACSAria flow cytometer, and 1 µm calibration beads were used for the flow rate calibration; autotrophic picoplankton are identified in plots of side scatter vs. red fluorescence. Heterotrophic bacterial abundance were obtained by subtracting autotrophic cell abundance from prokaryotic abundance. The flow cytometric data were analysed with the BD Accuri C6 software and FCS Express software.

DNA extraction, sequencing and analysis

One litre of seawater from each treatment was collected at 0, 18, 36, 48, and 120 h and filtered through 0.2 µm polycarbonate filters (Millipore, 47 mm diameter) under low pressure (less than 30 kPa), and the filters were stored at -80 °C until further analysis. Note that samples at 0 h were collected from only the control, and all the treatments shared the initial bacterial community structure of these samples. DNA was extracted from the samples using a previously described method (46).

The 16S rRNA gene V3-V4 region was amplified using a specific primer pair (341F-806R) (47) with a barcode. All PCRs were carried out with Phusion® High-Fidelity PCR Master Mix (New England Biolabs). Samples with bright main bands between 450 and 550 bp were chosen, and the band contents were purified with the Qiagen Gel Extraction Kit (Qiagen, Germany). The amplicons were paired-end sequenced using the HiSeq2500 platform (Illumina, Inc., San Diego, CA, USA). Sequences were assigned to each sample based on the barcode and truncated by cutting off the barcode and primer sequence. Sequence assembly was conducted with FLASH (V1.2.7)(48), and low-quality sequences were filtered under specific filtering conditions according to the QIIME (V1.7.0) quality control process (49). Chimeric sequences were detected with the Genomes Online Database (GOLD) using the UCHIME algorithm and then removed (50). Then, effective tags were finally obtained.

Sequence analysis was performed by UPARSE software (UPARSE v7.0.1001) (51). Sequences were assigned to the same OTUs at 97% similarity, and a representative sequence for each OTU was screened for further annotation. The OTU taxonomic

information was annotated using the RDP classifier (Version 2.2) (52) with the Greengenes database (53). The OTU abundance was normalized using a standard sequence number corresponding to the sample containing the fewest sequences. Subsequent analyses of alpha diversity and beta diversity were performed based on this output normalized data.

Microbial network analysis

A network was constructed following a previously published method (54), with some modification. OTUs were defined at 97% similarity, and those with a relative abundance above 0.1% in one sample that appeared in more than two samples of all treatments were selected. We calculated all possible Spearman's rank correlations between these OTUs. We considered a valid co-occurrence event to be a robust correlation if the Spearman's correlation coefficient was > 0.6 and a statistically significant *P*-value < 0.01 was present. The networks of each treatment were displayed separately with Gephi 0.9.2. To describe the topology of the network, some basic indices (node, edge, average degree, graph density, and others) were calculated.

Statistical analysis

Statistical analyses, including t-tests to examine the differences in the optical parameters of the generated DOM between Pro-exudate and Pro-vDOM, one-way ANOVAs to compare the differences in the heterotrophic bacterial abundance and DOM utilization rate, the calculation of the specific growth rate (μ) according to the general linear regression slope between the log-transformed bacterial abundance and growth time and univariate analysis to test the differences between the resulting μ

values, were performed using IBM SPSS Statistics 25.0 (IBM Corp., USA).

Nonmetric multidimensional scaling (NMDS) analysis for the bacterial community structure and the SIMPROF test for bacterial community similarity were performed with Primer 6 (PRIMER-E, UK). Bacterial relative abundance data were not transformed during NMDS and SIMPROF analysis. The R package (version 3.4.3) was used for the redundancy analysis (RDA analysis). Before RDA analysis, bacterial relative abundance data were transformed by Hellinger transformation, environmental factor (DOC, $S_{275-295}$, a_{280}, a_{254}, C1, C2, C3, C4, and C5) data were zero-centred and normalized, and covariability among environmental factors were examined using variance inflation factors (factors that least than 10 were selected). RDA analysis was conducted with vegan package via permutation test (999 permutations).

Data availability

The sequences reported in this paper have been deposited to the National Center for Biotechnology Information database under BioProject no. PRJNA644149 (releasing at November 7, 2020).

Results

DOM derived from *Prochlorococcus*

DOC concentrations of Pro-exudate and Pro-vDOM were much higher than that of Pro-medium (Table 1). The optical properties of DOM derived from *Prochlorococcus* were investigated using a UV-visible spectrophotometer and a spectrofluorometer. As shown in Table 1, the ultraviolet absorbance coefficient at 254 nm (a254) of Pro-vDOM (except P-HS2 lysate) were higher than those of Pro-exudate and the magnitude of this

trend varied between the different phage types used. Our data showed that the $S_{275-295}$ values of Pro-vDOM were significantly higher than those of Pro-exudate (t-test, $P<0.05$). This indicated that Pro-vDOM contained more LMW DOM than did Pro-exudate.

Pro-exudate and three Pro-vDOM shared similar fluorescence excitation-emission matrices (EEMs) (Figure 1). According to the EEMs of Pro-DOM, *Prochlorococcus* produced both protein-like (peak T) and humic-like fluorescent materials (peak A, C, M) through exudation and viral lysis (Table 1). Both Pro-exudate and Pro-vDOM showed the most prominent peaks at 250/466 nm (ex/em), which corresponded to previously defined "terrestrial humic-like" substances (peak A) (44). The fluorescence intensity of the peak at 335/404 nm (ex/em), which corresponds to marine humic-like materials (peak M) (44), was the second highest. Another humic-like peak assigned to peak C (ex/em 355/450 nm) appeared in all Pro-DOM. Compared to the peaks observed for Pro-medium, peak M and peak C were the most increased components. The fluorescence intensity of peak M of Pro-vDOM was significantly higher than that of Pro-exudate (t-test, $P<0.05$). In the protein-like region, one peak at ex/em 275/340 nm (peak T) was found in Pro-exudate and Pro-vDOM. Podovirus P-SSP7-mediated Pro-vDOM showed the highest fluorescence intensity for protein-like peak T.

The total dissolved amino acid (TDAA) analysis showed that Asp, Glu, Ala and Gly were the dominant amino acids in Pro-DOM (Table S2). Compared with those of Pro-medium, the DOC-normalized TDAA of Pro-DOM were significantly elevated, and the TDAA concentrations of the P-HS2 and P-SSP7 lysates were higher than those of Pro-

346 exudate, supporting the above shown $S_{275-295}$ results (Table 1). In addition, the total
347 concentration of the 14 amino acids of Pro-vDOM increased differently than did that
348 of Pro-exudate (Table S2). Together, our data showed that both the quantity and
349 quality of DOM were different between Pro-exudate and Pro-vDOM.

350 **Microbial utilization of DOM**

351 After DOM addition, the initial DOC concentration of all treatments ranged from
352 80.4 (Pro-medium treatment) to 89.4 µM (P-HS2 lysate treatment), corresponding to
353 DOC increases of 7.9% to 20.0% from the DOC concentration in the control (74.4 µM)
354 (Table S3). During the 120 h incubation experiment, the DOC concentration of the
355 control remained stable, while those of the DOM addition treatments rapidly
356 degraded in the first 18 h (Figure 2a). The amount of consumed DOC ranged from 3.6
357 µM to 8.6 µM in the first 18 h, corresponding to 4.5% to 9.6% of the initial DOC content
358 (Table S3). The DOC consumption ratio of Pro-vDOM was higher than that of Pro-
359 exudate at 18 h and 120 h.

360 Figure 2b displays the CDOM spectral slope $S_{275–295}$ of each treatment at a specific
361 sampling time during the incubation period. After DOM addition, the initial spectral
362 slopes ranked as follows: control > Pro-vDOM > Pro-exudate > Pro-medium. This result
363 suggested that the Pro-exudate treatment contained much more high-molecular-
364 weight DOM than did the Pro-vDOM treatments at the beginning of incubation. At the
365 end of the incubation, all DOM addition treatments had similar spectral slopes,
366 however, these slopes differed from those at the beginning (Figure 2b), hence resulting
367 in the spectral slope of Pro-vDOM decreasing more compared to that of Pro-exudate.

368 Five fluorescent components were identified using parallel factor analysis
369 (PARAFAC), including two protein-like and three humic-like components (Figure 3, left
370 panel). Components 1 and 5 (C1 and C5) were characterized as amino acid-like DOM
371 (44) and displayed relatively narrower emission spectra with maxima below 350 nm.
372 C1 displayed excitation maximum at 275 nm and one emission maximum at 332 nm,
373 which was similar to tryptophan-like peak T. C5 had an excitation/emission maximum
374 at 275/300 nm, similar to tyrosine-like peak B. Components 2, 3 and 4 (C2, C3 and C4)
375 were assigned to humic-like FDOM. C2 exhibited two peaks with excitation maxima at
376 255/365 nm and emission at 456 nm and was categorized as a combination of
377 terrigenous humic-like peaks A and C (44). C3 exhibited excitation maxima at <250 nm
378 with 368 nm emission. This matched with the C4 reported by Yamashita and colleagues
379 (55), and C4 is thought to be a microbe-derived humic-like component. The peak of C4
380 at 325/396 nm (ex/em) corresponded to marine humic-like fluorescence (peak M) (56).
381 Compared with that of the control, the initial fluorescence intensities of the
382 DOM-addition treatments increased to different degrees, and the most enriched of
383 the five components was C1 (Figure S2), indicating that the DOM quality of all
384 treatments changed after DOM addition. Since C5 contributes only a small part (10-
385 20%) of the protein-like fluorescence intensity, tryptophan-like C1 was selected as
386 representative of the protein-like components for subsequent analysis. The
387 fluorescence intensity of C1 sharply decreased over the entire incubation period in the
388 treatments but not in the control. After 120 h incubation, most (50-70%) C1 was
389 degraded in the Pro-medium and Pro-DOM treatments. Peaks A and C (referred to as

C2 in the incubation experiment) showed higher fluorescence intensities for Pro-DOM than for Pro-medium (Table 1), and the intensity of C2 had different increases from 24 or 36 h of incubation for different DOM treatments (Figure 3). These results suggest that C2 is produced not only by *Prochlorococcus* but also by heterotrophic bacteria under specific conditions. Moreover, C4 of the Pro-DOM treatment presented a higher fluorescence intensity than did that of the Pro-medium treatment and showed an intensity increase of 30-50%, though C4 represented only a small proportion of FDOM.

Growth of heterotrophic bacteria

During the course of the experiment, the heterotrophic bacterial abundances increased during the first phase, and later, this increase slowed and reached a stationary phase in all five treatments (Figure 4). In the control, the bacterial abundance increased from 3.5×10^5 cells mL^{-1} at 0 h to 8.4×10^5 cells mL^{-1} at 120 h. The bacterial abundances of the five treatments increased from an average of 3.1×10^5 cells mL^{-1} at the beginning to between 12×10^5 cells mL^{-1} and 15×10^5 cells mL^{-1} at the end, with a tendency of Pro-vDOM treatments showing higher bacterial abundances compared to the Pro-exudate treatment.

During the incubation, the growth curves of all treatments showed log growth and a stationary phase. The bacterial specific growth (μ) of the log-growth phase was estimated by the regression slope of the natural log-transformed bacterial abundance. The μ values of the Pro-DOM and Pro-medium treatments were significantly higher than that of the control (univariate analysis of variance, $p < 0.001$), and the μ values of the P-HS2 and P-SSP7 lysate treatments were significantly higher than that of the Pro-

412 exudate treatment (univariate analysis of variance, p = 0.007 and 0.016, respectively)
413 (Table S4). Although there was no significant difference, μ of the P-HM2 lysate
414 treatment (0.91 d^{-1}) was also higher than that of the Pro-exudate treatment (0.83 d^{-1})
415 (Table S4). After the stationary growth phase was reached, the bacterial abundance of
416 all Pro-vDOM treatments were significantly higher than that of the Pro-exudate
417 treatment (one-way ANOVA, P<0.05) (Table S5). Therefore, Pro-vDOM showed higher
418 bioavailability compared to Pro-exudate.

419 **Bacterial diversity and community composition**

420 During the incubation period, the alpha diversity (Shannon and Simpson indices)
421 of the bacterial community in the control and Pro-medium treatments remained
422 relatively constant, whereas those of the Pro-DOM treatments decreased sharply
423 during the first 48 h and then remained constant (Figure S3). It was also found that the
424 alpha diversity of Pro-vDOM was lower than that of Pro-exudate.

425 Alteromonadales, Rhodospirillales and SAR11 accounted for more than 50% of
426 the bacterial community throughout the experiment. The initial primary groups were
427 *Prochlorococcus* and *Pelagibacter*, and they shifted to *Nautella*, *Alteromonas*,
428 *Prochlorococcus*, and *Pelagibacter* at the end of the experiment in the control; to
429 *Alteromonas*, *Pelagibacter*, and *Thiomicrospira* in the Pro-medium samples; and to
430 *Nautella* and *Alteromonas* in the Pro-DOM samples (Figure 5). During the incubation,
431 the relative abundances of Rhodobacterales and Alteromonadales increased, while
432 those of the SAR11 clade and cyanobacteria decreased in all treatments. *Nautella* and
433 *Alteromonas* were the two groups that responded quickly to Pro-DOM addition and

434 predominated in the late period of the experiment in all DOM-amended treatments.

435 As shown in Figure 6, distinct changes in the bacterial community structure
436 mainly happened within 36 h, and then the bacterial community structure remained
437 stable. During the experimental period, the bacterial structure of the control had a
438 relatively small change compared with those of samples receiving DOM addition.
439 Compared with that of the Pro-medium treatment, the bacterial community structures
440 of Pro-DOM treatments had a distinct succession trajectory. A difference also existed
441 between the structures of Pro-exudate and Pro-vDOM treatments (especially for the
442 P-HS2 and P-SSP7 lysates). From 36 h, the similarity of the bacterial community
443 structure of the Pro-vDOM treatments were significantly different from that of the Pro-
444 exudate treatment at the corresponding sampling time (SIMPROF test, $p = 0.001$), and
445 the bacterial communities of the P-HS2 lysate and P-SSP7 lysate treatments were
446 similar (84.6%) but significantly different from that of the Pro-exudate treatment at
447 the 36 h and 48 h sampling points (SIMPROF test, $p = 0.001$). This indicated that the
448 Pro-exudate and Pro-vDOM treatments have different effects on microbial community
449 succession.

450 OTU-based microbial co-occurrence network analysis showed that most of the
451 highly connected OTUs were assigned to Alpha- and Gammaproteobacteria (Figure 7),
452 indicating that bacterial species in these two classes were key components of the
453 microbial community. DOM addition significantly increased the positive interactions
454 among microorganisms, and the graph density of the network of Pro-DOM treatments
455 was more than two times higher than that of the control and Pro-medium treatment

456 (Table S6). The increased interactions were mainly due to some specific OTUs that
457 belonged to Alphaproteobacteria in the Pro-medium and Pro-exudate treatments and
458 to Alphaproteobacteria, Gammaproteobacteria and cyanobacteria in the Pro-vDOM
459 treatments. The highly connected OTUs also differed among these DOM treatments.
460 In the Pro-medium treatment, the OTUs belonged to the SAR11 clade and
461 *Prochlorococcus*. *Rhodospirillaceae* and the SAR11 clade (except in the P-HM2 lysate
462 treatment) dominated in all Pro-DOM treatments, and *Prochlorococcus* also appeared
463 to have a close interaction with other OTUs in the Pro-vDOM treatments (except in the
464 P-HM2 lysate treatment). The negative interactions among microorganisms were also
465 affected by DOM addition (Table S6). There were small changes in the negative
466 interaction in the Pro-medium and Pro-exudate treatments compared with the control.
467 Compared with the Pro-exudate treatment, Pro-vDOM treatments had an apparent
468 increase in negative edges and nodes with negative interactions with other nodes.

469 ## Discussion

470 ### Viral lysis alters the quality of DOM released by *Prochlorococcus*

471 In this work, our DOC, CDOM, FDOM and amino acids data showed that viral lysis
472 altered the production and composition of DOM released by *Prochlorococcus*, which
473 is the most important photosynthetic picophytoplankton in the oligotrophic ocean.
474 This finding is consistent with those of previous studies based on other phytoplankton.
475 Viral infection alters the lipid composition of *Emiliania huxleyi* cellular materials (9)
476 and the composition of DOM released by *Micromonas pusilla* and *Synechococcus* (4,
477 13, 14). Treatments with Pro-vDOM, which contained intracellular materials of hosts,

478 resulted in a higher a_{254}, amino acid concentration and spectral slope $S_{275-295}$ compared
479 to treatment with Pro-exudate. During the incubation, Pro-vDOM treatments resulted
480 in a higher DOC degradation rate than the Pro-exudate treatment, and their $S_{275-295}$
481 values decreased more than that of the Pro-exudate treatment did (Table S3 and Figure
482 2b). Microbial degradation induces the decrease of $S_{275-295}$ as a result of LMW DOM
483 consumption (42). These results suggested that more labile LMW DOM was released
484 and then consumed in the Pro-vDOM treatments than in the Pro-exudate treatment.
485 In addition, the TDAA carbon yield, which indicates the degree of bioavailability of
486 DOM (57), of the Pro-vDOM treatments were much higher than that of the Pro-
487 exudate treatment at the beginning and close (0.8-1.1%) at the end of incubation
488 (Figure S4), resulting in the TDAA carbon yield of Pro-vDOM treatments decreasing
489 more than that of the Pro-exudate treatment. This indicated that Pro-vDOM has higher
490 bioavailability than Pro-exudate. This result was further supported by the finding that
491 the heterotrophic bacterial growth rate and abundance of the Pro-vDOM treatments
492 were significantly higher than those of the Pro-exudate treatment (Table S4, S5),
493 suggesting that Pro-vDOM was easier to convert to biomass than the Pro-exudate. It
494 is also possible that the labile DOM released by viral lysis may enhance the accessibility
495 of RDOM to bacterial remineralization due to the priming effect (58). Therefore, the
496 viral lysis of *Prochlorococcus* might fuel heterotrophic bacterial activity and,
497 subsequently, the microbial loop in vast oligotrophic oceans. In the initial viral shunt
498 concept (59), it was predicted that heterotrophic bacterial production is stimulated by
499 viral lysis products, i.e., by organic matter that enters the DOM pool and is hence not

transferred to higher trophic levels by grazing (5). Here, we present an additional interpretation, i.e., that viral lysis not only increases the concentration of the DOM pool, but also changes the quality of the DOM towards higher bioavailability.

Bacterial community fuelled by different sources of DOM

NMDS analysis showed that Pro-DOM had significant effects on the microbial community succession trajectories (Figure 6). Compared with the Pro-medium treatment, the Pro-DOM treatments had distinct community structures during the entire incubation period, suggesting that Pro-DOM had a significant role in shaping the microbial community. This is consistent with previously observed pronounced effects of phytoplankton-derived DOM (such as from diatoms and *Synechococcus*) on the bacterial community (60, 61). Importantly, we observed that the microbial community of the Pro-vDOM treatments had different succession trajectories compared with that of the Pro-exudate treatment (20). Previous works have suggested that the microbial community structure might be affected by both DOM quality and quantity (34-36). Our redundancy analysis (RDA) showed that the DOM composition could explain 50% of the total variation in the bacterial community composition, while the DOC concentration had a minor effect. This result was contrary to that reported by Sarmento and colleagues (36), who found that DOM quantity affects bacterial communities more than quality. A possible reason for this difference might be the relatively larger DOC concentration range (10, 30 and 100 μM) in their experiment than in our experiments. For example, high DOC concentrations could shift the bacterial community towards faster-growing OTUs (62). Therefore, the different responses of

522 the microbial community structure to Pro-vDOM and Pro-exudate treatments could
523 reflect differences in DOM quality due to providing specific ecological niches for
524 bacteria since similar initial DOC concentration were used in this study.

525 In addition, our work showed that vDOM produced by morphologically different
526 phages probably have diverging ecological roles, since they affected the bacterial
527 growth rate (Figure 4) and bacterial diversity (Figure S3) in different ways. These
528 differences may be related to DOM quality changes (such as the amino acid
529 composition and concentration and protein-like FDOM production) due to variations
530 in host-phage interactions. Thompson and colleagues demonstrated that marine
531 cyanophages carried and expressed auxiliary metabolic genes (AMGs) and may have
532 redirected the host carbon metabolism (63). It was reported that the three
533 cyanophages had different burst sizes and AMGs (64), which may lead to differences
534 in the quality of the organic matter in Pro-vDOM.

535 Furthermore, RDA analysis illustrated that specific microbial taxa were linked to
536 DOM characteristics (Figure 8). The absorption coefficient a280 and protein-like FDOM
537 C1 and C5 were positively correlated with the relative abundance of Alteromonadales,
538 which was one of the dominant groups in the incubation. These results are probably
539 explained by the fact that Alteromonadales was mainly responsible for CDOM removal
540 in the dark incubation. For C4, the humic-like FDOM component was positively related
541 to Rhodobacterales, indicating that Rhodobacterales might be the major biological
542 factor affecting the fate of humic-like DOM in dark conditions. Though both
543 Alteromonadales and Rhodobacterales were the dominant groups in this experiment,

544 the major roles of the two maybe differ in carbon processing. Alteromonadales have a
545 broad substrate preference relative to that of Rhodobacterales (65-67) and may apply
546 diverse complementary growth strategies to rapidly respond to external disturbances.
547 The coefficients a280, C1, and C5 closely correlated with early samples (in 18 h), and
548 C4 was correlated with later samples. This indicates that the early period was the DOM
549 removal and biomass accumulation phase and that the late phase was responsible for
550 humic-like DOM accumulation. This is supported by previous works showing that
551 bacteria incorporate labile DOM into biomass but respire low-quality DOM and
552 produce humic-like by-products (68, 69).

553 In microbial co-occurrence network analysis, positive relationships indicate co-
554 operation, co-colonization or niche overlap while negative relationships suggest
555 competition or prey–predator relationship (70). Compared with the control and Pro-
556 medium treatment, Pro-DOM addition significantly increased the positive relationship
557 among microorganisms (Table S6). The possible reason was that Pro-DOM is a complex
558 DOM mixture and needs additional microbial co-operation to be utilized. Furthermore,
559 the average degree of the network of Pro-vDOM was higher than that of Pro-exudate
560 (Table S6), indicating that denser interactions among species appeared in the Pro-
561 vDOM treatments than in the Pro-exudate treatment. In addition, negative
562 interactions increased in the Pro-vDOM treatments but not in the Pro-exudate
563 treatment. Detailed analysis showed that the negative interactions mainly happened
564 between the high-relative abundance OTUs (*Nautella*, *Alteromonas*, *Marinomonas*)
565 and other OTUs. These results suggested that these bacteria may have a greater

competitive pressure in Pro-vDOM treatments than in the Pro-exudate treatment, indicating that Pro-vDOM is likely more labile to oligotrophic microorganisms compared to Pro-exudate.

Implication: the impact of viral lysis on the production and transformation of DOM in the ocean

Peak M represents the primary humic-like material in *Prochlorococcus*-derived FDOM (Table 1), which is thought to be autochthonous humic-like DOM in the global ocean with a ubiquitously distributed microbial origin (44). The relatively high peak-M fluorescence intensity of the Pro-vDOM treatments indicated that viral lysis is a pathway that considerably contributes to the release of humic-like materials produced by *Prochlorococcus*. Previous global and regional surveys show that chlorophyll *a* is closely related to the distribution of peak M in oligotrophic epipelagic oceans (30, 71), where *Prochlorococcus* is the numerically dominant phytoplankton (22). In addition, *Prochlorococcus* has a similar vertical distribution pattern to that of peak M in the open ocean (30, 72). This indicates that viral lysis of *Prochlorococcus* is an important humic-like DOM source in the ocean. Considering the wide distribution and long turnover times (610 years) of peak M in the ocean (73), viral lysis of *Prochlorococcus* contributes to the recalcitrant DOM pool in the water column through microbial carbon pump (17).

Our study with isolates demonstrates that viral lysis is a source of labile and humic-like substances. It has been reported that cyanophage infection redirects host metabolism (63, 74), and it has been proposed that phage-encoded AMGs are responsible for this reprogramming (75). This suggests that viral infection plays a vital

588 role in affecting the host metabolism and the quality of host-released DOM and could
589 have contributed to our findings. Moreover, virus-induced mortality contributes
590 significantly to marine phytoplankton losses (5, 7). Therefore, we hypothesize that viral
591 lysis is also a potentially important source of labile and humic-like material in the global
592 ocean (4, 16).

593 **Methodological limitations**

594 Microcosm incubation is one of the approaches widely used to assess the
595 availability of DOM for natural microorganisms (12, 36, 76). In our experimental setup,
596 to eliminate grazing in the incubation, 0.8-μm filtration is used to remove predators
597 such as heterotrophic nanoflagellates and particles (12, 60, 77). Previous studies
598 showed that 1 μm or 0.8 μm filtration can eliminate all heterotrophic nanoflagellates
599 in most coastal and open regions of the South China Sea and the Atlantic Ocean (78,
600 79). However, the filtration inevitably results in a certain loss of bacterial cells and the
601 alteration of bacterial growth. To minimize these effects as much as possible, we used
602 a low filtration pressure and polycarbonate membranes instead of glass fiber
603 membranes, which can reduce the effect of filtration on the selective loss of bacteria
604 (80).

605 During *Prochlorococcus* DOM preparation, we used a standard culture medium,
606 Pro99 (32), to culture *Prochlorococcus* under continuous-light conditions for a better
607 cell yields. It is worth pointing out that the nutrients concentrations (N/P) of Pro99
608 medium were higher than those in natural sea water (32 and references therein). So
609 far, there is no evidence indicating that the physiological and ecological characteristics

610 of *Prochlorococcus* grown in Pro99 are different from those *in situ*. For example, their
611 temperature optima and light requirements are consistent with their distribution in
612 the ocean (72). However, it is unknown whether the modification of these culture
613 conditions affect the *Prochlorococcus* DOM composition released during viral infection.
614 In addition, in accordance with previous studies (60, 65, 76), the present study added
615 a relatively lower percentage of DOC into the incubation systems compared with
616 environmental conditions. However, the DOM amendments should be higher than the
617 amount of DOC released by *Prochlorococcus* in *in situ* environments. Based on the
618 available data regarding *Prochlorococcus* viral mortality rate (8, 24, 25), cellular carbon
619 content (81) and DOC exuded rate (3), it is estimated that *Prochlorococcus* contributed
620 DOC of less than 1 µmol-C L^{-1} d^{-1} under *in situ* conditions. Therefore, the addition of
621 DOM may impact and will probably stimulate, bacterial growth. The possible
622 differences in the quantity and quality of the *Prochlorococcus* DOM between our
623 microcosm and natural environments need to be considered when applying our
624 conclusions to biogeochemical studies. Moreover, viral lysis contributes to the
625 production of both dissolved and particulate (cell debris) organic matter. Most studies,
626 including the present one, have focused on DOM (12, 16, 21). To obtain a complete
627 view of viral-driven production and transformation of organic matter, more
628 investigations on organic particles generated during lysis are needed.

629 **Conclusion**

630 In summary, we demonstrated that viral lysis altered the quality and quantity of
631 DOM released by *Prochlorococcus*, and hence, viral lysates of *Prochlorococcus* might

be a pathway that considerably contributes to marine CDOM and humic-like DOM pools. These results are an important step towards linking laboratory studies and large-scale oceanographic surveys by potentially allowing to identify sources of vDOM in the ocean. *Prochlorococcus* lysates were more labile compared to the *Prochlorococcus* exudate and shaped the microbial community with different succession trajectories. Under the conditions of global climate change, the distribution of *Prochlorococcus* might broaden, its abundance might increase (22), and the contribution of viral lysis to phytoplankton mortality might be enhanced (8). The data suggest that viral infection of *Prochlorococcus* may play an important role in shaping DOM cycling and pooling in oligotrophic oceans.

Acknowledgements

This work was supported by the National Natural Science Foundation of China projects (41861144018 to N. J., 91951209 to R. Z., 41876083 to W. G., 41676059 and 41890801 to X. L), the Research Grants Council of the Hong Kong Special Administrative Region, China (16102317) to Q. Z., and the 111 Program of Xiamen University to M.G.W. We thank the captain, crew, and scientists aboard the R/V Shiyan III, led by chief scientist Jia Sun, for their support during the cruise. Thanks to Qiaoyun Qin for assistance in using R software (RDA analysis) and Adobe Illustrator (Figure S1), Jing Xu for her technical support during FDOM data analysis, and three anonymous reviewers whose comments improved the manuscript.

Competing interests

The authors declare no competing interests.

Additional information

Supplementary information is available at the Applied and Environmental Microbiology's website.

References

1. Field CB, Behrenfeld MJ, Randerson JT, Falkowski P. 1998. Primary Production of the Biosphere: Integrating Terrestrial and Oceanic Components. Science 281:237.
2. Falkowski PG, Raven JA. 2007. Aquatic Photosynthesis in Biogeochemical Cycles, p 364-410. *In* Falkowski PG, Raven JA (ed), Aquatic Photosynthesis, Second Edition ed. Princeton University Press.
3. Bertilsson S, Berglund O, Pullin MJ, Chisholm SW. 2005. Release of dissolved organic matter by Prochlorococcus. Vie Et Milieu-Life and Environment 55:225-231.
4. Lønborg C, Middelboe M, Brussaard CPD. 2013. Viral lysis of Micromonas pusilla: impacts on dissolved organic matter production and composition. Biogeochemistry 116:231-240.
5. Fuhrman JA. 1999. Marine viruses and their biogeochemical and ecological effects. Nature 399:541-548.
6. Thornton DCO. 2014. Dissolved organic matter (DOM) release by phytoplankton in the contemporary and future ocean. European Journal of Phycology 49:20-46.
7. Suttle CA, Chan AM, Cottrell MT. 1990. Infection of phytoplankton by viruses and reduction of primary productivity. Nature 347:467.
8. Mojica KDA, Huisman J, Wilhelm SW, Brussaard CPD. 2016. Latitudinal variation in virus-induced mortality of phytoplankton across the North Atlantic Ocean. ISME J 10:500-513.
9. Evans C, Pond DW, Wilson WH. 2009. Changes in Emiliania huxleyi fatty acid profiles during infection with E. huxleyi virus 86: physiological and ecological implications. Aquatic Microbial Ecology 55:219-228.
10. Chrost RH, Faust MA. 1983. Organic carbon release by phytoplankton: its composition and utilization by bacterioplankton. Journal of Plankton Research 5:477-493.
11. Chen W, Wangersky PJ. 1996. Rates of microbial degradation of dissolved organic carbon from phytoplankton cultures. Journal of Plankton Research 18:1521-1533.
12. Zhao Z, Gonsior M, Schmitt-Kopplin P, Zhan Y, Zhang R, Jiao N, Chen F. 2019. Microbial transformation of virus-induced dissolved organic matter from picocyanobacteria: coupling of bacterial diversity and DOM chemodiversity. ISME J doi:10.1038/s41396-019-0449-1.
13. Ma XF, Coleman ML, Waldbauer JR. 2018. Distinct molecular signatures in dissolved organic matter produced by viral lysis of marine cyanobacteria. Environmental Microbiology 0.
14. Zhao Z, Gonsior M, Luek J, Timko S, Ianiri H, Hertkorn N, Schmitt-Kopplin P, Fang XT, Zeng QL, Jiao NZ, Chen F. 2017. Picocyanobacteria and deep-ocean fluorescent dissolved organic matter share similar optical properties. Nature Communications 8:15284.
15. Fiore CL, Longnecker K, Soule MCK, Kujawinski EB. 2015. Release of ecologically relevant metabolites by the cyanobacterium *Synechococcus* elongatus CCMP 1631. Environmental Microbiology 17:3949-3963.
16. Gobler CJ, Hutchins DA, Fisher NS, Cosper EM, Sanudo-Wilhelmy SA. 1997. Release and

bioavailability of C, N, P, Se, and Fe following viral lysis of a marine chrysophyte. Limnology and Oceanography 42:1492-1504.

17. Jiao N, Herndl GJ, Hansell DA, Benner R, Kattner G, Wilhelm SW, Kirchman DL, Weinbauer MG, Luo TW, Chen F, Azam F. 2010. Microbial production of recalcitrant dissolved organic matter: long-term carbon storage in the global ocean. Nature Reviews Microbiology 8:593-599.

18. Azam F, Fenchel T, Field JG, Gray JS, Meyerreil LA, Thingstad F. 1983. The Ecological Role of Water-Column Microbes in the Sea. Marine Ecology Progress Series 10:257-263.

19. Haaber J, Middelboe M. 2009. Viral lysis of Phaeocystis pouchetii: Implications for algal population dynamics and heterotrophic C, N and P cycling. ISME J 3:430-441.

20. Sheik AR, Brussaard CPD, Lavik G, Lam P, Musat N, Krupke A, Littmann S, Strous M, Kuypers MMM. 2014. Responses of the coastal bacterial community to viral infection of the algae Phaeocystis globosa. Isme Journal 8:212-225.

21. Fang X, Liu Y, Zhao Y, Chen Y, Liu R, Qin Q-L, Li G, Zhang Y-Z, Chan W, Hess WR, Zeng Q. 2019. Transcriptomic responses of the marine cyanobacterium Prochlorococcus to viral lysis products. Environmental Microbiology 21:2015-2028.

22. Flombaum P, Gallegos JL, Gordillo RA, Rincon J, Zabala LL, Jiao NAZ, Karl DM, Li WKW, Lomas MW, Veneziano D, Vera CS, Vrugt JA, Martiny AC. 2013. Present and future global distributions of the marine Cyanobacteria Prochlorococcus and Synechococcus. Proceedings of the National Academy of Sciences of the United States of America 110:9824-9829.

23. Partensky F, Garczarek L. 2010. Prochlorococcus: Advantages and Limits of Minimalism. Annual Review of Marine Science 2:305-331.

24. Pasulka AL, Samo TJ, Landry MR. 2015. Grazer and viral impacts on microbial growth and mortality in the southern California Current Ecosystem. Journal of Plankton Research 37:320-336.

25. Baudoux AC, Veldhuis MJW, Witte HJ, Brussaard CPD. 2007. Viruses as mortality agents of picophytoplankton in the deep chlorophyll maximum layer during IRONAGES III. Limnology and Oceanography 52:2519-2529.

26. Lea-Smith DJ, Biller SJ, Davey MP, Cotton CAR, Sepulveda BMP, Turchyn AV, Scanlan DJ, Smith AG, Chisholm SW, Howe CJ. 2015. Contribution of cyanobacterial alkane production to the ocean hydrocarbon cycle. Proceedings of the National Academy of Sciences of the United States of America 112:13591-13596.

27. Becker JW, Berube PM, Follett CL, Waterbury JB, Chisholm SW, DeLong EF, Repeta DJ. 2014. Closely related phytoplankton species produce similar suites of dissolved organic matter. Frontiers in Microbiology 5.

28. Bouman HA, Ulloa O, Scanlan DJ, Zwirglmaier K, Li WKW, Platt T, Stuart V, Barlow R, Leth O, Clementson L, Lutz V, Fukasawa M, Watanabe S, Sathyendranath S. 2006. Oceanographic basis of the global surface distribution of Prochlorococcus ecotypes. Science 312:918-921.

29. Hansen AM, Kraus TEC, Pellerin BA, Fleck JA, Downing BD, Bergamaschi BA. 2016. Optical properties of dissolved organic matter (DOM): Effects of biological and photolytic degradation. Limnology and Oceanography 61:1015-1032.

30. Catalá TS, Álvarez-Salgado XA, Otero J, Iuculano F, Companys B, Horstkotte B, Romera-Castillo C, Nieto-Cid M, Latasa M, Morán XAG, Gasol JM, Marrasé C, Stedmon CA, Reche I. 2016. Drivers of fluorescent dissolved organic matter in the global epipelagic ocean. Limnology and Oceanography 61:1101-1119.

31. Yamashita Y, Tanoue E. 2008. Production of bio-refractory fluorescent dissolved organic matter in the ocean interior. Nature Geoscience 1:579-582.
32. Moore LR, Coe A, Zinser ER, Saito MA, Sullivan MB, Lindell D, Frois-Moniz K, Waterbury J, Chisholm SW. 2007. Culturing the marine cyanobacterium Prochlorococcus. Limnology and Oceanography-Methods 5:353-362.
33. Wong GTF, Ku T-L, Mulholland M, Tseng C-M, Wang D-P. 2007. The SouthEast Asian Time-series Study (SEATS) and the biogeochemistry of the South China Sea—An overview. Deep Sea Research Part II: Topical Studies in Oceanography 54:1434-1447.
34. Docherty KM, Young KC, Maurice PA, Bridgham SD. 2006. Dissolved Organic Matter Concentration and Quality Influences upon Structure and Function of Freshwater Microbial Communities. Microbial Ecology 52:378-388.
35. Logue JB, Lindström ES. 2008. Biogeography of Bacterioplankton in Inland Waters. Freshwater Reviews 1:99-114.
36. Sarmento H, Morana C, Gasol JM. 2016. Bacterioplankton niche partitioning in the use of phytoplankton-derived dissolved organic carbon: quantity is more important than quality. ISME J 10:2582-2592.
37. Lindroth P, Mopper K. 1979. High performance liquid chromatographic determination of subpicomole amounts of amino acids by precolumn fluorescence derivatization with o-phthaldialdehyde. Analytical Chemistry 51:1667-1674.
38. Li X, Liu Z, Chen W, Wang L, He B, Wu K, Gu S, Jiang P, Huang B, Dai M. 2018. Production and Transformation of Dissolved and Particulate Organic Matter as Indicated by Amino Acids in the Pearl River Estuary, China. Journal of Geophysical Research: Biogeosciences 123:3523-3537.
39. Yamashita Y, Cory RM, Nishioka J, Kuma K, Tanoue E, Jaffe R. 2010. Fluorescence characteristics of dissolved organic matter in the deep waters of the Okhotsk Sea and the northwestern North Pacific Ocean. Deep-Sea Research Part Ii-Topical Studies in Oceanography 57:1478-1485.
40. Spencer RGM, Hernes PJ, Ruf R, Baker A, Dyda RY, Stubbins A, Six J. 2010. Temporal controls on dissolved organic matter and lignin biogeochemistry in a pristine tropical river, Democratic Republic of Congo. Journal of Geophysical Research: Biogeosciences 115:n/a-n/a.
41. Guo W, Yang L, Zhai W, Chen W, Osburn CL, Huang X, Li Y. 2014. Runoff-mediated seasonal oscillation in the dynamics of dissolved organic matter in different branches of a large bifurcated estuary—The Changjiang Estuary. Journal of Geophysical Research: Biogeosciences 119:776-793.
42. Helms JR, Stubbins A, Ritchie JD, Minor EC, Kieber DJ, Mopper K. 2008. Absorption spectral slopes and slope ratios as indicators of molecular weight, source, and photobleaching of chromophoric dissolved organic matter. Limnology and Oceanography 53:955-969.
43. Stedmon CA, Bro R. 2008. Characterizing dissolved organic matter fluorescence with parallel factor analysis: a tutorial. Limnology and Oceanography-Methods 6:572-579.
44. Coble PG. 1996. Characterization of marine and terrestrial DOM in seawater using excitation emission matrix spectroscopy. Marine Chemistry 51:325-346.
45. Marie D, Partensky F, Vaulot D, Brussaard C. 1999. Enumeration of Phytoplankton, Bacteria, and Viruses in Marine Samples. Current Protocols in Cytometry 10:11.11.1-11.11.15.
46. Zhang R, Xia X, Lau SCK, Motegi C, Weinbauer MG, Jiao N. 2013. Response of bacterioplankton community structure to an artificial gradient of pCO_2 in the Arctic Ocean. Biogeosciences 10:3679-3689.

47. Klindworth A, Pruesse E, Schweer T, Peplies J, Quast C, Horn M, Glöckner FO. 2013. Evaluation of general 16S ribosomal RNA gene PCR primers for classical and next-generation sequencing-based diversity studies. Nucleic Acids Research 41:e1-e1.
48. Magoč T, Salzberg SL. 2011. FLASH: fast length adjustment of short reads to improve genome assemblies. Bioinformatics 27:2957-2963.
49. Caporaso JG, Kuczynski J, Stombaugh J, Bittinger K, Bushman FD, Costello EK, Fierer N, Peña AG, Goodrich JK, Gordon JI, Huttley GA, Kelley ST, Knights D, Koenig JE, Ley RE, Lozupone CA, McDonald D, Muegge BD, Pirrung M, Reeder J, Sevinsky JR, Turnbaugh PJ, Walters WA, Widmann J, Yatsunenko T, Zaneveld J, Knight R. 2010. QIIME allows analysis of high-throughput community sequencing data. Nature Methods 7:335.
50. Edgar RC, Haas BJ, Clemente JC, Quince C, Knight R. 2011. UCHIME improves sensitivity and speed of chimera detection. Bioinformatics 27:2194-2200.
51. Edgar RC. 2013. UPARSE: highly accurate OTU sequences from microbial amplicon reads. Nature Methods 10:996.
52. Wang Q, Garrity GM, Tiedje JM, Cole JR. 2007. Naïve Bayesian Classifier for Rapid Assignment of rRNA Sequences into the New Bacterial Taxonomy. Applied and Environmental Microbiology 73:5261-5267.
53. DeSantis TZ, Hugenholtz P, Larsen N, Rojas M, Brodie EL, Keller K, Huber T, Dalevi D, Hu P, Andersen GL. 2006. Greengenes, a Chimera-Checked 16S rRNA Gene Database and Workbench Compatible with ARB. Applied and Environmental Microbiology 72:5069-5072.
54. Barberán A, Bates ST, Casamayor EO, Fierer N. 2011. Using network analysis to explore co-occurrence patterns in soil microbial communities. The Isme Journal 6:343.
55. Yamashita Y, Panton A, Mahaffey C, Jaffé R. 2011. Assessing the spatial and temporal variability of dissolved organic matter in Liverpool Bay using excitation–emission matrix fluorescence and parallel factor analysis. Ocean Dynamics 61:569-579.
56. Kothawala DN, von Wachenfeldt E, Koehler B, Tranvik LJ. 2012. Selective loss and preservation of lake water dissolved organic matter fluorescence during long-term dark incubations. Science of The Total Environment 433:238-246.
57. Shen Y, Fichot CG, Benner R. 2012. Dissolved organic matter composition and bioavailability reflect ecosystem productivity in the Western Arctic Ocean. Biogeosciences 9:4993-5005.
58. Bianchi TS, Thornton DCO, Yvon-Lewis SA, King GM, Eglinton TI, Shields MR, Ward ND, Curtis J. 2015. Positive priming of terrestrially derived dissolved organic matter in a freshwater microcosm system. Geophysical Research Letters 42:5460-5467.
59. Wilhelm SW, Suttle CA. 1999. Viruses and Nutrient Cycles in the Sea - Viruses play critical roles in the structure and function of aquatic food webs. Bioscience 49:781-788.
60. Landa M, Blain S, Harmand J, Monchy S, Rapaport A, Obernosterer I. 2018. Major changes in the composition of a Southern Ocean bacterial community in response to diatom-derived dissolved organic matter. FEMS Microbiology Ecology 94:fiy034-fiy034.
61. Tada Y, Suzuki K. 2016. Changes in the community structure of free-living heterotrophic bacteria in the open tropical Pacific Ocean in response to microalgal lysate-derived dissolved organic matter. FEMS Microbiology Ecology 92.
62. Zhang R, Weinbauer M, Tam Y, Qian P-Y. 2013. Response of bacterioplankton to a glucose gradient in the absence of lysis and grazing. FEMS microbiology ecology 85.
63. Thompson LR, Zeng Q, Kelly L, Huang KH, Singer AU, Stubbe J, Chisholm SW. 2011. Phage

auxiliary metabolic genes and the redirection of cyanobacterial host carbon metabolism. Proceedings of the National Academy of Sciences of the United States of America 108:E757-E764.

64. Frois-Moniz K. 2014. Host/Virus Interactions in the Marine Cyanobacterium Prochlorococcus. Ph.D Thesis. Massachusetts Institute of Technology, Cambridge, MA.

65. Nelson CE, Carlson CA. 2012. Tracking differential incorporation of dissolved organic carbon types among diverse lineages of Sargasso Sea bacterioplankton. Environmental Microbiology 14:1500-1516.

66. Taylor JD, Cunliffe M. 2017. Coastal bacterioplankton community response to diatom-derived polysaccharide microgels. Environmental Microbiology Reports 9:151-157.

67. Gómez-Consarnau L, Lindh MV, Gasol JM, Pinhassi J. 2012. Structuring of bacterioplankton communities by specific dissolved organic carbon compounds. Environmental Microbiology 14:2361-2378.

68. Ogawa H, Amagai Y, Koike I, Kaiser K, Benner R. 2001. Production of refractory dissolved organic matter by bacteria. Science 292:917-920.

69. Fasching C, Behounek B, Singer GA, Battin TJ. 2014. Microbial degradation of terrigenous dissolved organic matter and potential consequences for carbon cycling in brown-water streams. Scientific Reports 4:4981.

70. Faust K, Raes J. 2012. Microbial interactions: from networks to models. Nature Reviews Microbiology 10:538.

71. Martínez-Pérez AM, Catalá TS, Nieto-Cid M, Otero J, Álvarez M, Emelianov M, Reche I, Álvarez-Salgado XA, Arístegui J. 2019. Dissolved organic matter (DOM) in the open Mediterranean Sea. II: Basin-wide distribution and drivers of fluorescent DOM. Progress in Oceanography 106:93-106.

72. Biller SJ, Berube PM, Lindell D, Chisholm SW. 2015. Prochlorococcus: the structure and function of collective diversity. Nature Reviews Microbiology 13:13-27.

73. Catalá TS, Reche I, Fuentes-Lema A, Romera-Castillo C, Nieto-Cid M, Ortega-Retuerta E, Calvo E, Alvarez M, Marrase C, Stedmon CA, Alvarez-Salgado XA. 2015. Turnover time of fluorescent dissolved organic matter in the dark global ocean. Nature Communications 6.

74. Kaplan A. 2016. Cyanophages: Starving the Host to Recruit Resources. Current Biology 26:R511-R513.

75. Hurwitz BL, U'Ren JM. 2016. Viral metabolic reprogramming in marine ecosystems. Current Opinion in Microbiology 31:161-168.

76. Sharma AK, Becker JW, Ottesen EA, Bryant JA, Duhamel S, Karl DM, Cordero OX, Repeta DJ, DeLong EF. 2014. Distinct dissolved organic matter sources induce rapid transcriptional responses in coexisting populations of *Prochlorococcus*, Pelagibacter and the OM60 clade. Environmental Microbiology 16:2815-2830.

77. Dadaglio L, Dinasquet J, Obernosterer I, Joux F. 2018. Differential responses of bacteria to diatom-derived dissolved organic matter in the Arctic Ocean. Aquatic Microbial Ecology 82:59-72.

78. Jürgens K, Gasol JM, Vaqué D. 2000. Bacteria–flagellate coupling in microcosm experiments in the Central Atlantic Ocean. Journal of Experimental Marine Biology and Ecology 245:127-147.

79. Zhang R, Weinbauer MG, Qian P-Y. 2007. Viruses and flagellates sustain apparent richness and reduce biomass accumulation of bacterioplankton in coastal marine waters. Environmental

Microbiology 9:3008-3018.

80. Gasol J, M. , Morán X, A. G. 1999. Effects of filtration on bacterial activity and picoplankton community structure as assessed by flow cytometry. Aquatic Microbial Ecology 16:251-264.

81. Bertilsson S, Berglund O, Karl DM, Chisholm SW. 2003. Elemental composition of marine Prochlorococcus and Synechococcus: Implications for the ecological stoichiometry of the sea. Limnology and Oceanography 48:1721-1731.

877 **Figures**

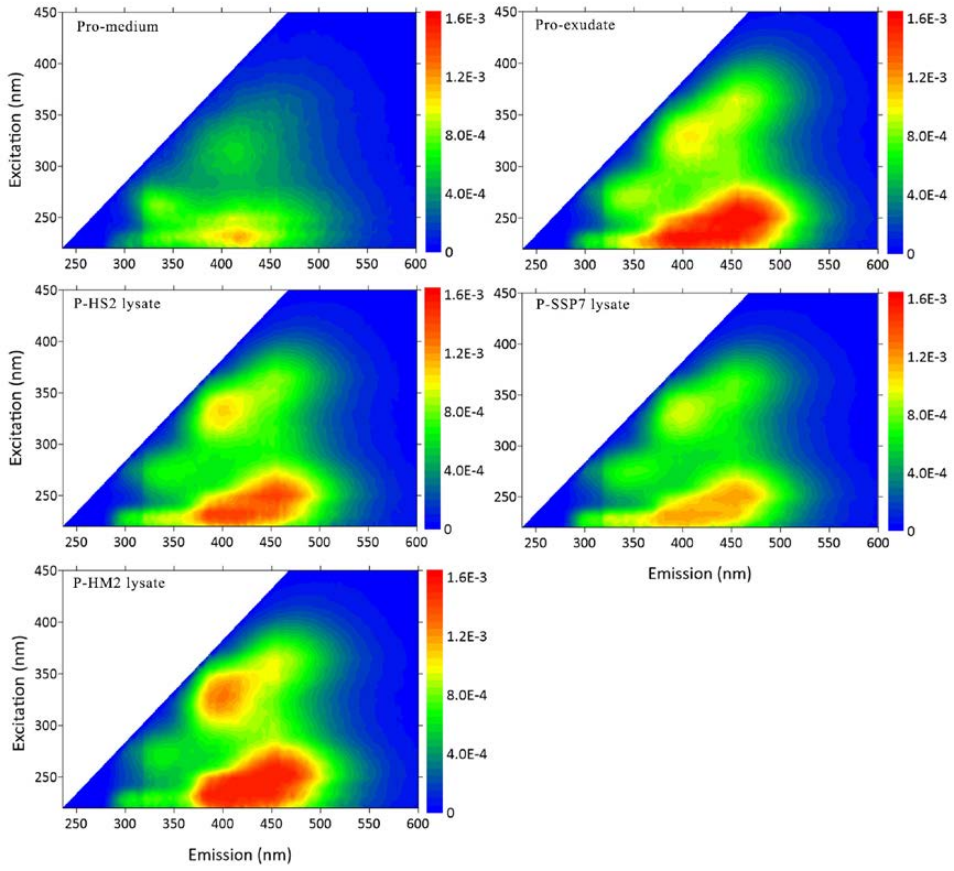

878

879 Figure 1. Viral lysis enhanced the production of fluorescent DOM derived from

880 *Prochlorococcus*. The fluorescence intensity of the excitation-emission matrix of the

881 five generated DOM were normalized to the DOC concentration. Unit: L μmol-C^{-1} R.U.

882 The scale bar along each figure represents the fluorescence intensity. Please note the

883 scale bar differences between different graphs.

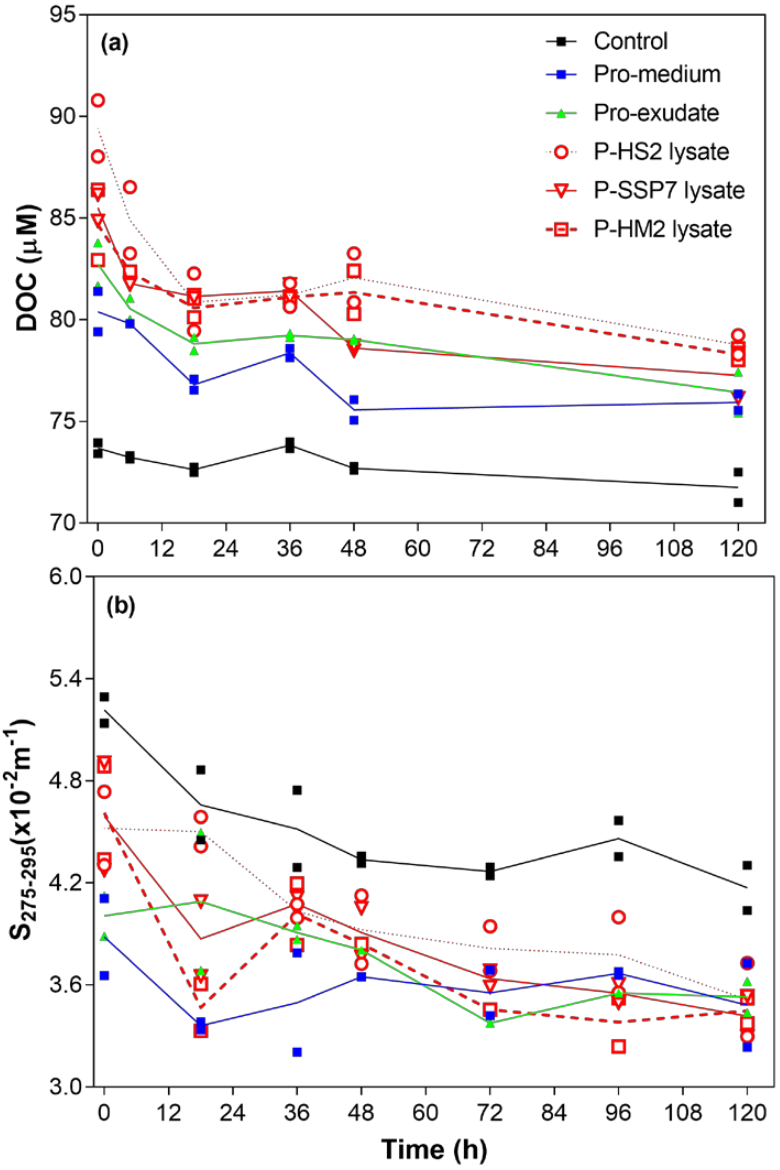

884

885 Figure 2. Changes in DOM quantity and quality after incubation with *Prochlorococcus*

886 exudate and lysate produced by different viruses. (a) Microbial utilization of different

887 DOC derived from *Prochlorococcus* DOM; (b) the DOM spectral slope $S_{275–295}$, which is

888 typically related to DOM molecular weight, at specific sampling times for each DOM

889 treatment. The value of each replicate and the trend line of each treatment are shown.

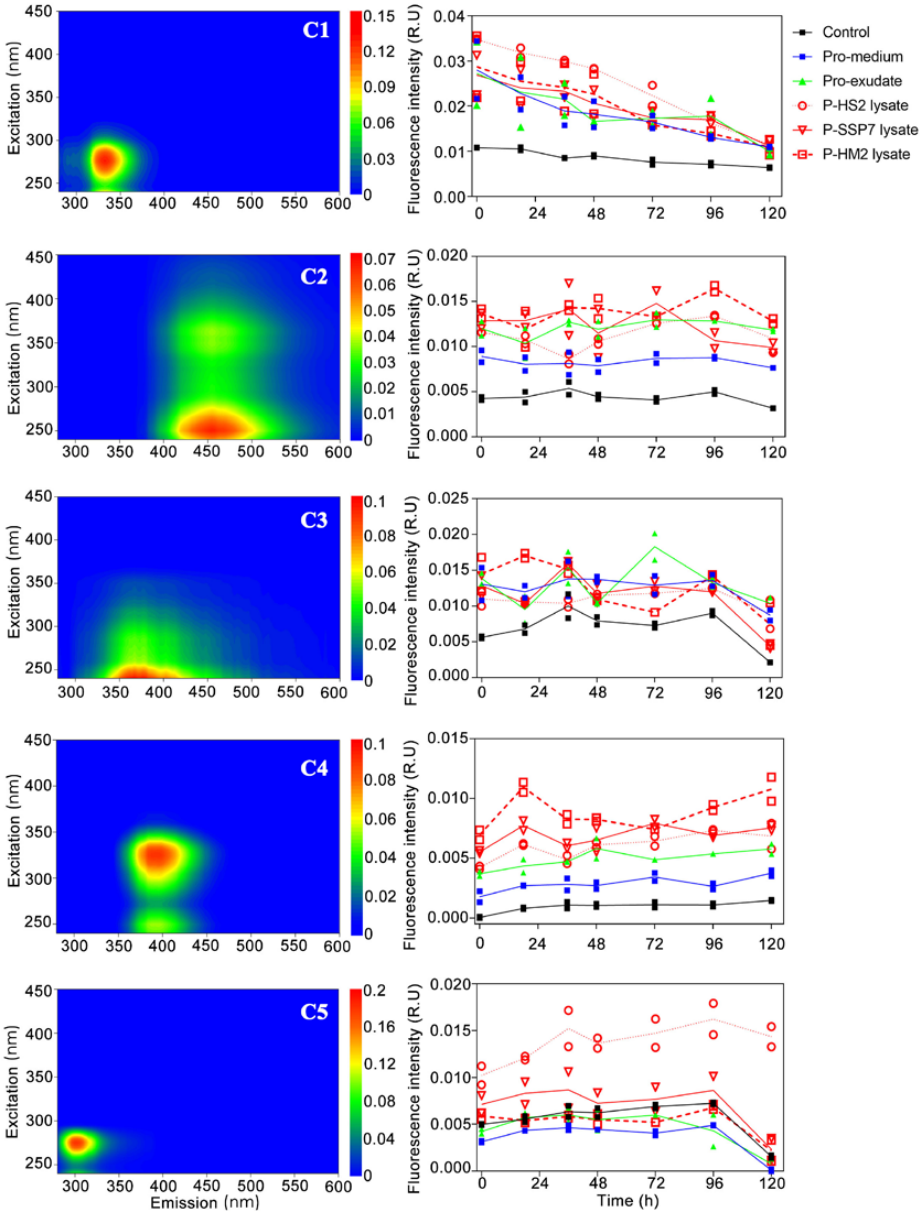

890

891 Figure 3. Microbial utilization of different components of fluorescent DOM derived

892 from *Prochlorococcus*. Left panels, excitation-emission matrix contours of the five

893 fluorescent components (C1-C5) identified using PARAFAC analysis; right panels, the

894 corresponding FDOM component changed after incubation with different types of

895 *Prochlorococcus*-derived DOM. The value of each replicate and the trend line of each

896 treatment are shown.

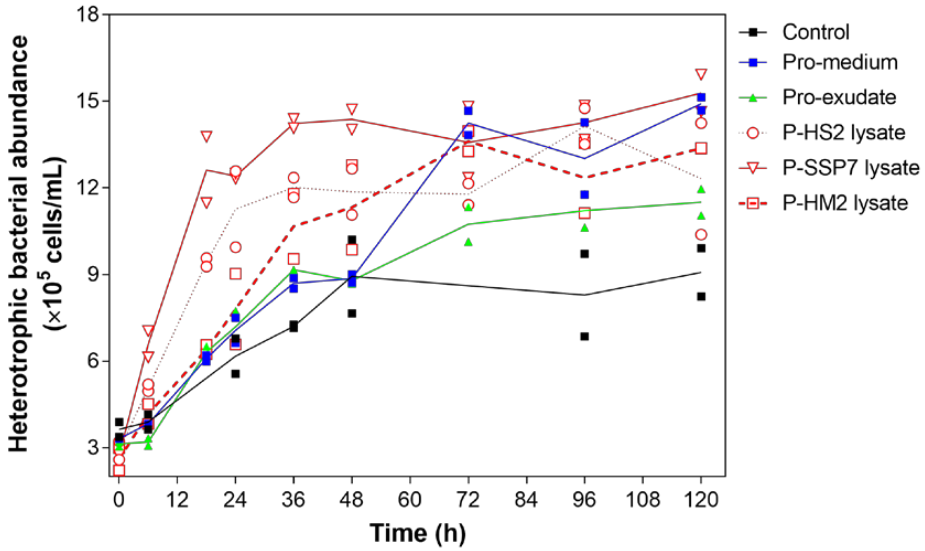

897

898 Figure 4. Growth of heterotrophic bacterioplankton after incubation with

899 *Prochlorococcus*-derived DOM. The value of each replicate and the trend line of each

900 treatment are shown.

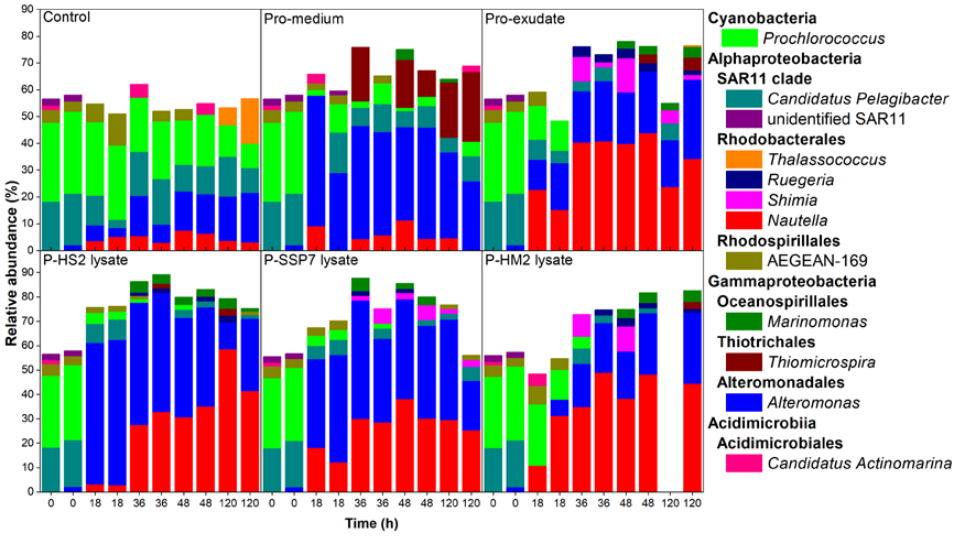

Figure 5. The response of the microbial community structure (genus level) to *Prochlorococcus*-derived DOM. The top 5 abundant genera in at least one sample were selected. Two bars having the same x-axis indicates replicates, and two replicates of each Pro-DOM treatment at each sampling time data are shown here (except the P-HM2 lysate at 120 h, which had only one sample). The names of the treatments are shown in the corresponding figures.

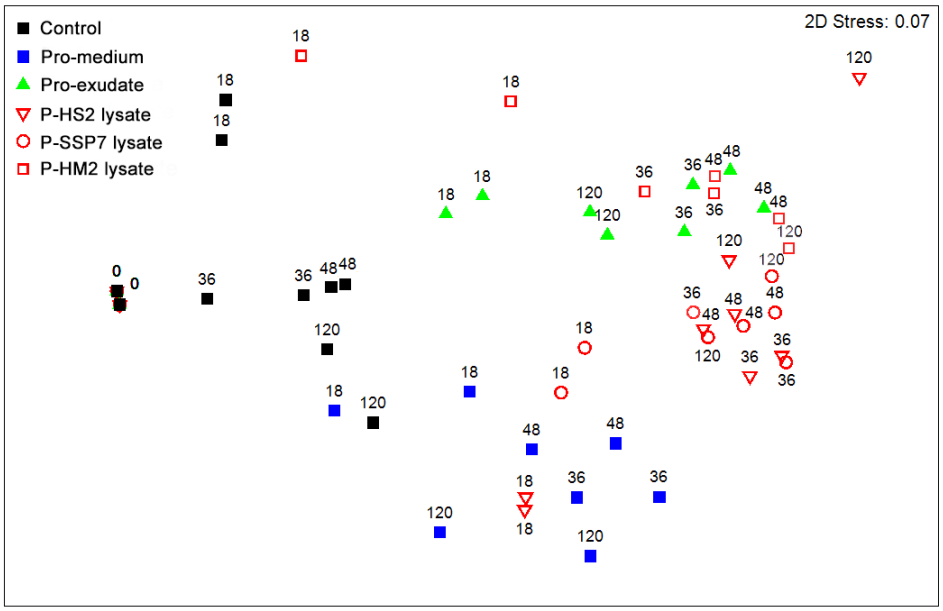

908

909 Figure 6. Effect of *Prochlorococcus*-derived DOM on the succession of the bacterial
910 community structure, as revealed by nonmetric multidimensional scaling (NMDS)
911 analysis. The number on each symbol indicates the sampling time of each treatment,
912 and all treatments at each sampling time had two replicates (except the P-HM2 lysate
913 treatment at 120 h), as shown by two of each symbol having the same number.

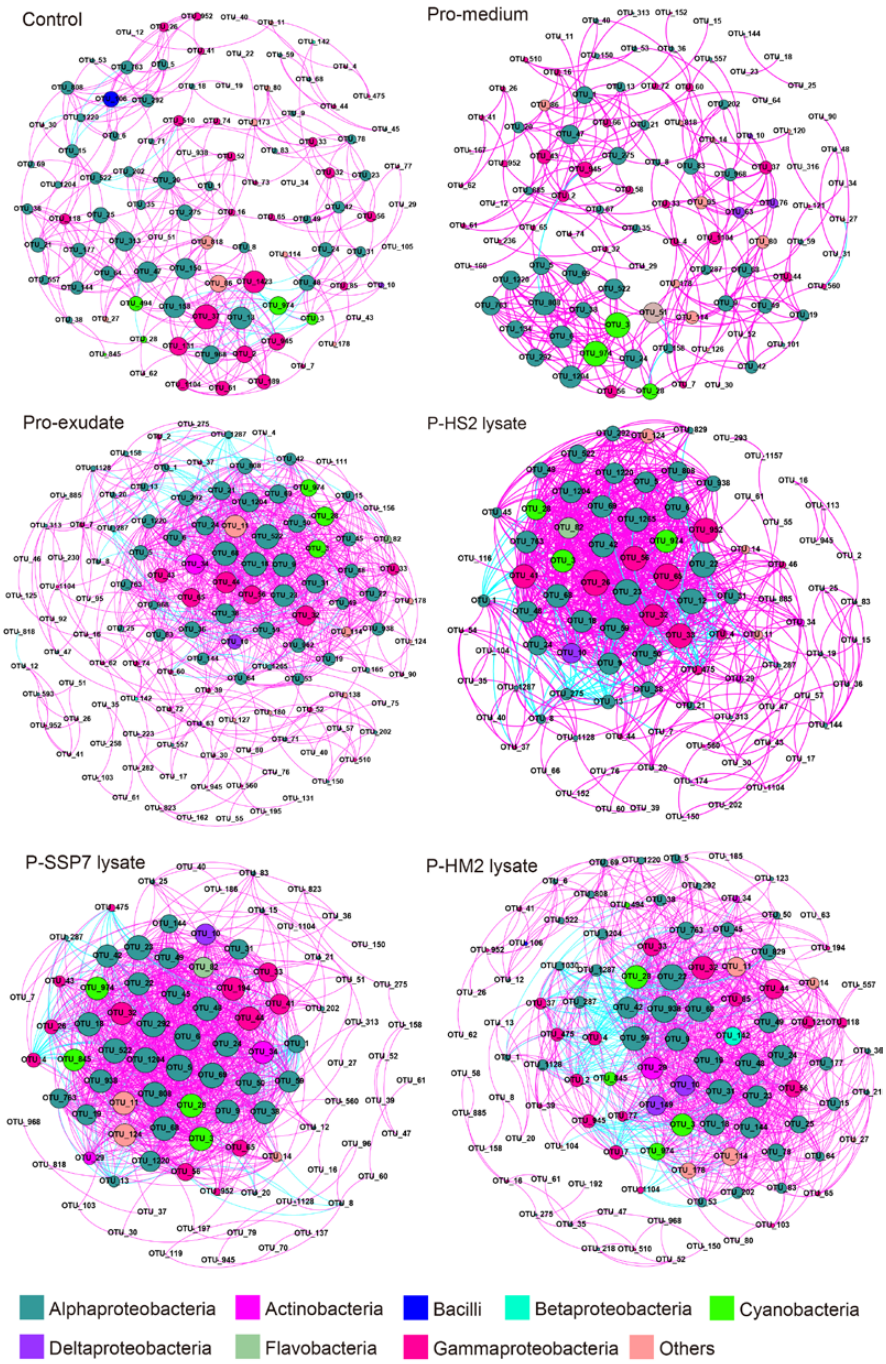

914

915 Figure 7. OTU-based network revealing intense interaction among microbial

916 communities after incubation with *Prochlorococcus*-derived DOM. Red and cyan

917 connections represent positive and negative interactions, respectively.

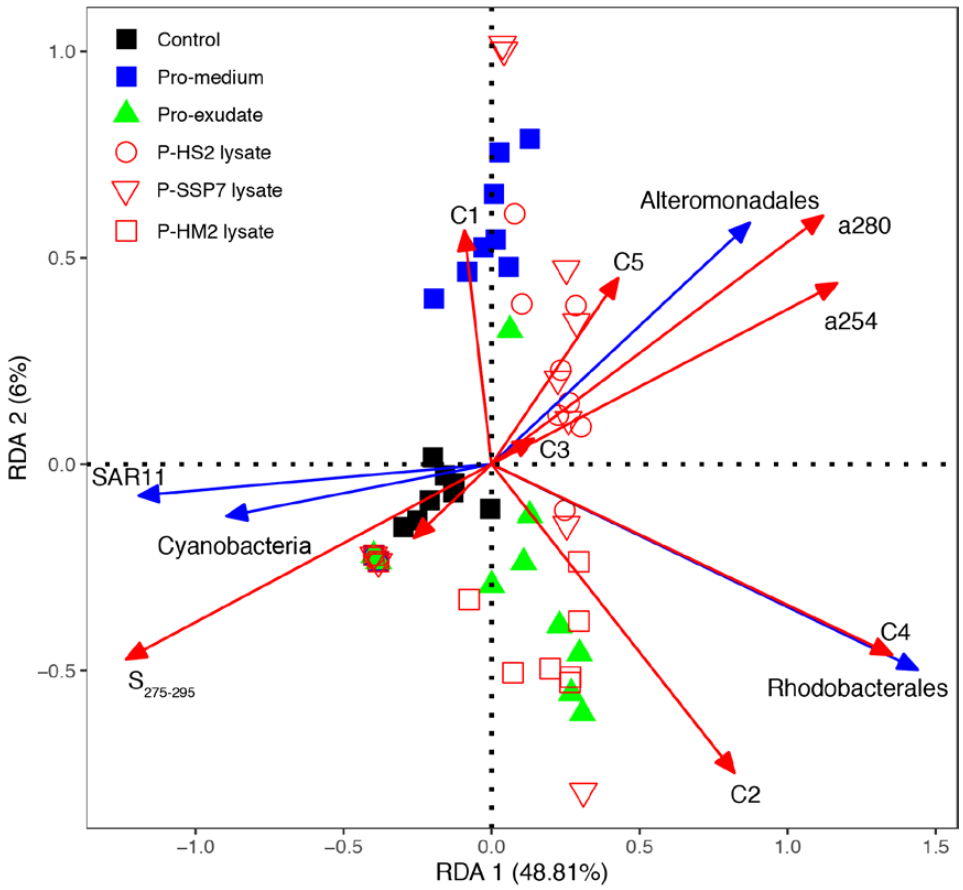

Figure 8. Redundancy analysis illustrating specific bacterial groups closely linked to specific DOM characteristics. a_{280}, C2, C5, $P = 0.001$; C4, $P = 0.01$; $S_{275\text{-}295}$, C3, $p < 0.05$; DOC, C1, a_{254}, $P > 0.05$. Only the bacterial groups that were significantly correlated with DOM indices are shown in the figure. All the bacterial community samples (without sampling times) are also presented in the figure. The samples located on the positive section of the second axis of the RDA figure are the early samples (at 18 or 36 h) of this incubation.

926 **Tables**

927 Table 1. The DOC concentration and optical properties of the DOM derived from Prochlorococcus. The FDOM components (C1-C5), as identified by

928 PARAFAC modelling, are shown with the corresponding FDOM components (peaks A, M, C and T) identified by the peak-picking method. The data

929 shown are the means of two replicates.

DOM source	DOC (μM)	a_{254} (m^{-1})	$S_{275-295}$* (10^{-2} nm^{-1})	Humic like components (R.U.)						Protein like components (R.U.)		
				peak A	C2	peak M *	C4 *	peak C	C3	peak T	C1	C5
				250/466	255/456	335/404	325/396	355/450	<250/368	270/342	275/332	275/300
Pro-medium	160.9	-	-	0.19	0.12	0.09	0.08	0.06	0.13	0.15	0.13	0.04
Pro-exudate	234.0	3.37	2.88	0.36	0.36	0.22	0.22	0.20	0.19	0.25	0.24	0.08
P-HS2 lysate	259.5	3.65	3.29	0.37	0.34	0.27	0.26	0.21	0.14	0.19	0.18	0.08
P-SSP7 lysate	319.0	4.77	4.27	0.35	0.36	0.29	0.28	0.23	0.18	0.26	0.26	0.08
P-HM2 lysate	244.4	5.08	3.80	0.38	0.38	0.30	0.30	0.22	0.17	0.19	0.19	0.06

930 *, represent the significant difference between Pro-exudate and Pro-vDOM, t-test (double tailed), $P<0.05$.